Ab initio phonon dispersions of face centered cubic Pb: effects of spin–orbit coupling

2008 J. Phys.: Condens. Matter 20 445202

(http://iopscience.iop.org/0953-8984/20/44/445202)

IOP PUBLISHING JOURNAL OF PHYSICS: CONDENSED MATTER

J. Phys.: Condens. Matter **20** (2008) 445202 (6pp) doi:10.1088/0953-8984/20/44/445202

Ab initio phonon dispersions of face centered cubic Pb: effects of spin–orbit coupling

Andrea Dal Corso

SISSA, Via Beirut 2/4, 34014 Trieste, Italy
and
INFM-DEMOCRITOS, Trieste, Italy

Received 25 July 2008, in final form 10 September 2008
Published 30 September 2008
Online at stacks.iop.org/JPhysCM/20/445202

Abstract

I present the *ab initio* phonon dispersions of face centered cubic Pb calculated within the framework of density functional perturbation theory, with plane waves and a fully relativistic ultrasoft pseudopotential which includes spin–orbit coupling effects. I find that, within the local density approximation, the theory gives phonon frequencies close to the experimental inelastic neutron scattering data. Many of the anomalies present in these dispersions are well reproduced by the fully relativistic pseudopotential theory and can be shown to appear only for small values of the smearing parameter that controls the sharpness of the Fermi surface.

The phonon dispersions of face centered cubic Pb (fcc-Pb) were measured accurately in the 1960s by means of inelastic neutron scattering [1], but since then their theoretical interpretation has been a challenge and is still a source of debate and surprises. Quite recently, an unexpected coincidence between the binding energy of the superconducting electron pairs and the energy of the phonon at a Kohn anomaly [2] was found experimentally, by resonant spin-echo neutron spectroscopy, for fcc-Pb and fcc-Nb [3]. In both cases, *ab initio* calculations could not reproduce or explain the anomalies [3]. Apparently Pb seems to be a relatively simple metal, with a Fermi surface similar to a free electron sphere perturbed at the Bragg planes by the lattice potential and several attempts to get its phonon dispersions with model pseudopotentials have been reported [4–6]. In practice, even modern *ab initio* methods have found difficulties with the lattice dynamics of fcc-Pb due to the presence of several anomalies and to the small values of the interatomic force constants that make more evident the errors due to the numerical and physical approximations.

The interatomic force constants of Pb, due mainly to sp electrons, are quite small compared to the interatomic force constants of noble and transition metals in which d electrons contribute to the binding. For instance, at the zone-boundary point X ($\mathbf{q} = (1, 0, 0)$),[1] the longitudinal (L) phonon is 62 cm^{-1} in Pb [1], 154 cm^{-1} in Au [7] and 193 cm^{-1} in Pt [8]. Moreover, the phonon dispersions of Pb contain sudden jumps of the slope in the frequency–wavevector curves. Some of these jumps have been classified as Kohn anomalies [9], and in some cases it has been relatively easy to support this assignment by finding a nesting vector that joins two parts of the Fermi surface with parallel tangents, but in other cases the explanation was much less straightforward. For instance it is still not clear whether the dips of the transverse (T) and L branches at the X point are Kohn anomalies because an appropriate nesting vector has not been easy to identify. Actually the presence of spin-density waves was proposed to explain this feature [10]. In several papers, it has been pointed out that Pb with an atomic charge $Z = 82$ is a heavy element for which relativistic and spin–orbit effects are quite large and might play a role in the description of the lattice dynamics [4, 5]. Some model pseudopotential calculations addressed this issue but could not entirely reproduce the experiment [11].

Pioneering first-principles calculations of the lattice dynamics of Pb were presented in the 1990s [12–14]. In [12], density functional perturbation theory (DFPT) [15] in a plane wave pseudopotential (PP) context was applied to the problem. The PP [16] was constructed with 6s and 6p valence electrons and accounting for relativistic effects at the scalar relativistic (SR) level [17]. The results were quite encouraging. The main anomaly visible in the L branch along the Σ line (from Γ ($\mathbf{q} = (0, 0, 0)$) to K ($\mathbf{q} = (0.75, 0.75, 0)$) to X) was

[1] Throughout the paper, $\mathbf{q}$ vectors are expressed in units of $2\pi/a_0$, where a_0 is the fcc lattice constant.

reproduced accurately. At the X point the L phonon frequency was overestimated by only 10 cm^{-1} while the frequency of the transverse (T) mode was overestimated by about 5 cm^{-1}. Moreover, it was observed that the L phonon frequency was decreasing by reducing the smearing parameter that controls the sharpness of the Fermi surface, suggesting that a Kohn anomaly not exactly reproduced by the calculation might explain the dip at X in the Pb dispersion. The quantitative error in the frequencies was attributed to the frozen core approximation due to the presence of 5d electrons in the core.

A successive linear muffin-tin orbital (LMTO) all-electron calculation removed the frozen core approximation [13], and found that the L frequency at X was well reproduced. Only the discrepancy of the T frequency at X could not be solved and no anomaly was found. Both the all-electron and the PP calculations were within the local density approximation (LDA) although with two different formulae for the correlation energy of the free electron gas. The theoretical lattice constants turned out to be quite different, probably due both to the different treatment of the 5d electrons and to the slightly different functional. Another plane wave PPs [14] calculation performed in the same period using the Wigner interpolation formula for the exchange and correlation energy and the nonlinear core correction [18] to account for the 5d electrons was in substantial agreement with the results of [12], although the lattice constant was closer to the experiment as in the all-electron calculation.

More recently the phonon dispersions of Pb have been revisited by a frozen phonon approach based on the projector augmented wave (PAW) method [19]. This calculation found that the LDA overestimates both the L and the T mode frequencies at X as in [12]. The generalized gradient approximation (GGA) provided overall better dispersions but significant differences with experiment still remained [19].

So far all *ab initio* calculations of the Pb phonon dispersions have been performed within the SR approximation. It is therefore worthwhile to estimate, using modern first-principles methods, the effects of the spin–orbit coupling on the dispersions. Recently, I have generalized DFPT for lattice dynamics to the fully relativistic (FR) ultrasoft PPs [20], which account for spin–orbit coupling close to the nucleus where it is expected to be important. For Au, the inclusion of spin–orbit coupling was found to be irrelevant for the description of the phonon dispersions. However for Pt, where there is a clearly visible Kohn anomaly in the T_1 phonon branch along the Σ line, the SR and the FR PPs differed significantly close to the Kohn anomaly and the FR-PP dispersion turned out to be closer to experiment.

The purpose of this paper is to apply the above theory to fcc-Pb and in particular to study some anomalies of its phonon dispersions. I find that, within the local density approximation (LDA), a FR-PP with 5d, 6s and 6p valence electrons gives generally lower frequencies than a SR-PP made with the same cut-off radii and the same electronic configuration. The phonon frequencies of fcc-Pb are so low that spin–orbit effects, although on an absolute scale quite small, significantly improve the agreement with the experimental results. The main anomalies visible in the phonon dispersions of Pb are well reproduced by the method and can be shown to be compatible with Kohn anomalies because they appear only for sufficiently small values of the smearing parameter that determines the sharpness of the Fermi surface.

Ultrasoft PPs [21] for Pb have been generated according to a modified Rappe, Rabe, Kaxiras and Joannopoulos (RRKJ) scheme [22] with three Bessel functions, following the method of [23]. The 5d, 6s and 6p electrons are considered as valence electrons.[2] Two different PPs are generated. In the FR-PP [24], the large components of the solutions of the radial Dirac equation are taken as reference wavefunctions, while in the SR-PP, the solutions of the Koelling and Harmon SR equation [17] are taken as reference. The numerical results are obtained within the LDA using the Perdew and Zunger parameterization of the exchange and correlation energy [25]. A kinetic energy cut-off of 30 Ryd is used for expanding the wavefunctions while the augmentation charges are expanded up to 300 Ryd. For the Brillouin zone (BZ) integration, uniform $N_k \times N_k \times N_k$ **k**-point meshes are used. The presence of a Fermi surface is dealt with by the smearing technique of [26] with a smearing parameter $\sigma = 0.01$ Ryd. Initially, the dynamical matrices have been computed with $N_k = 24$ on an $8 \times 8 \times 8$ **q**-point grid and a Fourier interpolation has been used to obtain complete phonon dispersions. Due to the presence of several anomalies, this grid, sufficient to give a general picture of the phonon dispersions, is not sufficient to reproduce their fine details. In order to compare theoretical results and experiment, instead of trying a larger calculation with a denser **q**-point grid, I have calculated the phonon frequencies directly using DFPT along special symmetry lines: the Δ line, from Γ to X, the Σ line described above and the Λ line, from Γ to L ($\mathbf{q} = (0.5, 0.5, 0.5)$).[3] In these calculations, the BZ sampling has been done mainly with $N_k = 32$ and, in a few cases, with $N_k = 40$ (see below). Finally, note that the results have been corrected to account for the acoustic sum rule[4]. This procedure affects by more than 1 cm^{-1} only the phonon frequencies from Γ up to $\mathbf{q} = (0.05, 0.05, 0)$ along the Σ line, and the two points $\mathbf{q} = (0.025, 0.025, 0.025)$ and $\mathbf{q} = (0.05, 0, 0)$.

In table 1, I report the equilibrium lattice constants, bulk moduli, and cohesive energies of fcc-Pb obtained from a fit with the Murnaghan equation of the total energy as a function of the volume for the two PPs used in this paper. In the same table, I report also some theoretical values present in the literature together with the extrapolated $T = 0$ K experimental values given in [19]. At $T = 300$ K the experimental lattice constant is 9.35 au [28]. The SR and FR lattice constants are very close to each other and differ by 0.5% from experiment, in good agreement with the recent SR-PAW results [19]. The FR

[2] I used as reference the all-electron configuration $5d^{10}6s^26p^2$ for the SR-PP and $5d^4_{3/2}5d^6_{5/2}6s^2_{1/2}6p^2_{1/2}$ for the FR-PP. The core radii (in au) of our PPs are: 5d, $5d_{3/2}$, $5d_{5/2}$ (1.7, 2.2), 6p, $6p_{1/2}$ (2.9), $6p_{3/2}$ (3.0). The 6s potential pseudized before $r_c = 2.2$ has been taken as the local potential. Two values of the core radii indicate a channel which has been pseudized with the ultrasoft scheme. In such cases, the first value is the norm conserving core radius and the second is the ultrasoft one. Nonlinear core corrections are not included in the PPs.

[3] The discretization was $((i-1)\Delta\zeta, 0, 0)$ along the Δ line, $(((i-1)\Delta\zeta, (i-1)\Delta\zeta, 0))$ along Σ and $(((i-1)\Delta\zeta, (i-1)\Delta\zeta, (i-1)\Delta\zeta))$ along Λ where i is an integer and $\Delta\zeta = 0.025$ ($\Delta\zeta = 0.05$) along Σ and Λ (Δ).

[4] I used the form of the acoustic sum rule reported (equation (81)) in [27].

Table 1. Calculated LDA lattice constant (a_0), bulk modulus (B_0), and cohesive energy (E_c) for fcc-Pb. The atomic energy is obtained at the magnetic ground state ($5d^{10}6s^26p^2$) in the SR case and at the nonmagnetic ground state ($5d^4_{3/2}5d^6_{5/2}6s^2_{1/2}6p^2_{1/2}$) in the FR case. Experimental data have been extrapolated to the zero-temperature limit in [19].

fcc-Pb	a_0 (au)	B_0 (kbar)	E_c (eV/atom)
FR-PP	9.23	496	2.5
SR-PP	9.23	520	3.7
SR-PP (BHS semilocal) [12]	9.01	516	
SR-PAW [19]	9.21	530	
Expt [19] ($T \to 0$)	9.27	490	2.02[a]

[a] Reference [29].

Table 2. LDA frequencies of fcc-Pb calculated at selected points of the BZ. All frequencies are in cm^{-1}. Experimental data, at $T = 100$ K, are from [1].

fcc-Pb	X_T	X_L	W_1	W_2	L_T	L_L
SR	41	71	55	62	34	80
FR	28	63	49	55	30	73
Expt	30	62	49	57	30	73

bulk modulus is slightly lower than the SR one but closer to the experimental value. The phonon calculations are performed at the theoretical lattice constant reported in table 1. As already noted in [29], although 5d electrons are quite low in energy (centered at 16.9 eV below the Fermi level in the SR case and at 18.2 and 15.7 eV in the FR case), the inclusion of 5d electrons in the valence has a significant effect on the lattice constant. The PPs [16] used in [12] and built using only the 6s and 6p orbitals give a lattice constant that is 2.8% smaller than that from experiment. The effect on the bulk modulus is however less important. Finally, we note that the cohesive energy calculated with the FR US-PP is about 1.2 eV lower than the SR one which, on the other hand, is in agreement with the value given in [29]. This large difference is due to the reference atomic configuration used in the two cases. Actually the SR magnetic ground state of the Pb atom has higher energy than the FR nonmagnetic ground state because it can be obtained with FR orbitals partially occupying the high energy $6p_{3/2}$ levels, which are instead empty in the FR ground state where the two 6p electrons are in the twofold-degenerate $6p_{1/2}$ level. The SR and FR energy difference between the fcc and bcc structures at the $T = 0$ K experimental fcc volume is much smaller. We find 2 mRyd (fcc is more stable than bcc) in the FR case and a slightly higher value, 3 mRyd, in the SR case, in agreement with [30].

The phonon frequencies calculated using the SR and the FR PPs at a few selected points of the BZ are compared with experiment in table 2. The FR frequencies are lower than the corresponding SR frequencies. At the L point the difference is about 4 cm^{-1} (T) and 7 cm^{-1} (L), while at X the difference is larger (13 cm^{-1} (T) and 8 cm^{-1} (L)). The FR frequencies agree with the experiment within a few cm^{-1} while the SR frequencies are higher.

The FR LDA phonon dispersions of fcc-Pb are shown in figure 1 along the main high symmetry lines of the BZ of the fcc lattice and compared to the experimental inelastic

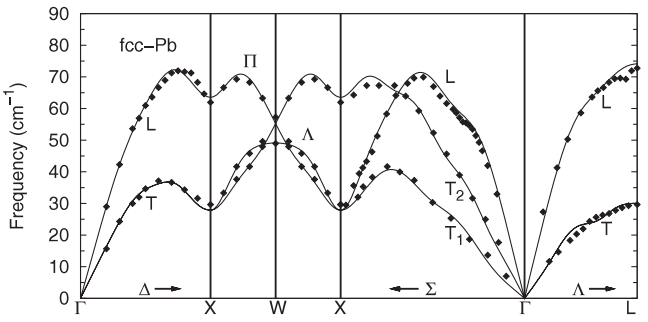

Figure 1. LDA phonon dispersions (solid lines) for fcc-Pb calculated at the theoretical lattice constant compared to inelastic neutron scattering data (solid diamonds) at $T = 100$ K [1]. A FR-PP with 5d, 6s and 6p valence electrons and an $8 \times 8 \times 8$ Fourier interpolation grid have been used.

neutron scattering data measured at 100 K. The experimental frequencies plotted in figure 1 along the Δ, Σ and Λ lines are taken from tables I and II of [1] and have a quoted error of ± 0.7 cm^{-1} or ± 1 cm^{-1}, while the points shown in the X–W–X direction have been extracted from figure 5 of [1] and have probably slightly larger errors. Our calculation is at $T = 0$ K, but for Pb this is not a severe approximation. At $T = 100$ K, anharmonic effects are expected to be quite small, the most important one being the thermal lattice expansion. As calculated in [19], the lattice constant expands by about 0.1% passing from $T = 0$ to 100 K. Zero-point motion, which expands the lattice constant further, gives an even smaller contribution [19].

Overall our theoretical FR dispersions improve the agreement between theory and experiment with respect to previous SR calculations [12, 14, 19], but the shape of these dispersions is not sufficiently converged with respect to the size of the Fourier grid. In [1], it was observed that the interatomic force constants necessary to fit the fcc-Pb phonon dispersions extend to a large number of neighbors, a fact attributed to the large dips in the phonon frequencies at the X point. In our Fourier interpolated dispersions, the flat T_2 branch close to the X point is not reproduced and a spurious oscillation appears in the T branch along Λ. There is no anomaly in the L branch along Λ and the oscillations of the T_1 branch along Σ seem to be opposite to the oscillations of the experimental points. If compared with the detailed spin-echo measurements [3] the deviations of the phase velocity from the average value of the interpolated T_1 branch would be opposite to the experimental ones.

The phonon dispersions, calculated directly using DFPT and with $N_k = 32$, are shown in figures 2 and 3. In these dispersions the T_2 branch close to the X point is flat and the oscillation in the T branch along the Λ line disappears. Moreover, an anomaly appears in the L branch along Λ, as well as a sudden change of slope in the L branch close to X in the Σ line. Along the Δ line the DFPT phonon frequencies reproduce the experiment much better than the interpolated curve and no new anomaly becomes visible. From these two figures we can also estimate the error due to the BZ sampling away from the anomalies. Actually the small discrepancies

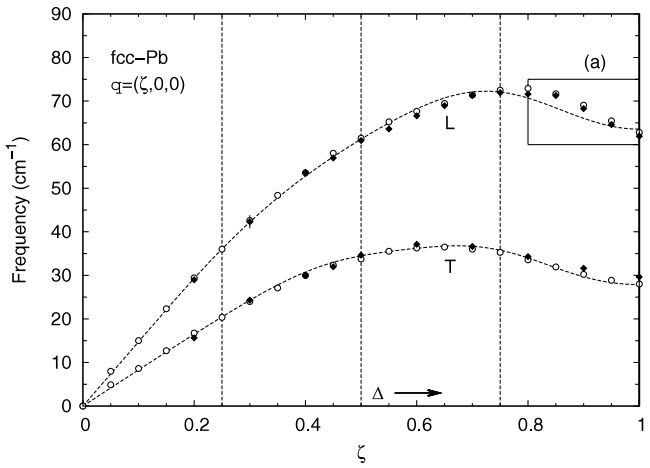

Figure 2. LDA phonon frequencies calculated using DFPT (empty circles) for fcc-Pb compared to inelastic neutron scattering data (solid diamonds) at $T = 100$ K [1]. The dashed lines show the phonon dispersions of figure 1. The dispersions are shown along the Δ line. Dashed vertical lines mark the positions of the points of the Fourier grid. An enlarged view of the dispersion inside the square (a) is presented in figure 7. A maximum error bar (± 1.5 cm^{-1}) is shown on one experimental point.

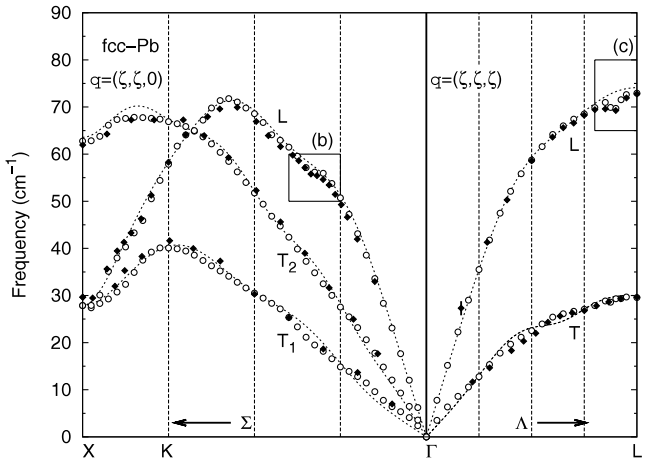

Figure 3. Phonon dispersions of fcc-Pb along the Σ and Λ lines. The symbols are the same as in figure 2. Enlarged views of the dispersions inside the squares (b) and (c) are shown in figures 5 and 6, respectively.

between the interpolated dispersions and the calculated DFPT points on the Fourier grid (indicated by dashed vertical lines in figures 2 and 3) are due to the different N_k used in the two calculations. At the L point in the L branch, where the discrepancy is particularly large, there is a difference of about 1 cm^{-1}.

Let us now focus on the dispersions contained within rectangles in figures 2 and 3 which present anomalies in the frequency–wavevector curves. In order to discuss these anomalies, it is useful to look at the Fermi surface. A contour plot of the Fermi surface in the $(1\bar{1}0)$ plane is shown in figure 4 and it is calculated both with the FR and with the SR PPs. In the same figure, I plot also the surface of a free electron gas with a density of four electrons per fcc-Pb unit cell. In the $(1\bar{1}0)$ plane

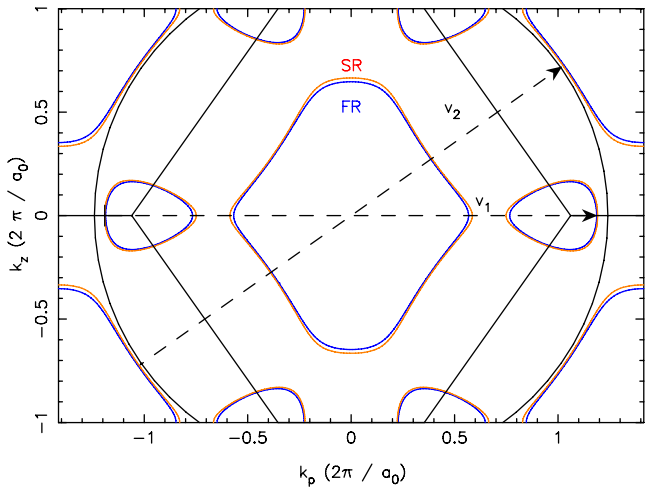

Figure 4. Fermi surface of fcc-Pb in the $(1\bar{1}0)$ plane. Both the SR (red line) and the FR (blue line) Fermi surfaces are shown. Two nesting vectors $\mathbf{v}_1 = -(0.32, 0.32, 0) + (2, 2, 0)$ and $\mathbf{v}_2 = (0.45, 0.45, 0.45) + (1, 1, 1)$ that correspond to the anomalies in figures 5 and 6 are indicated. The circle shows, in the extended zone, the Fermi sphere of a free electron gas with four valence electrons in the unit cell of fcc-Pb. $k_p = \mathrm{sgn}(k_x)\sqrt{k_x^2 + k_y^2}$.

(This figure is in colour only in the electronic version)

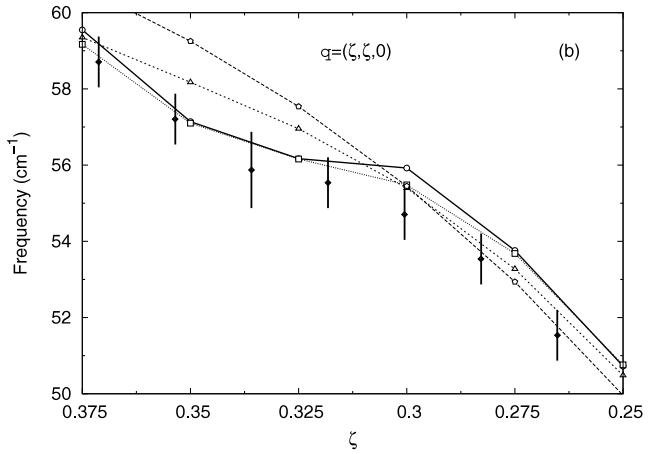

Figure 5. Enlarged view of the FR phonon dispersion of the L branch close to the point $\mathbf{q} = (0.32, 0.32, 0)$ (square (b) in figure 3) along the Σ line. The dispersion is calculated with several values of the smearing parameter σ which controls the sharpness of the Fermi surface. $\sigma = 0.1$ Ryd (pentagons), $\sigma = 0.05$ Ryd (triangles), $\sigma = 0.02$ Ryd (squares), $\sigma = 0.01$ Ryd (circles). Neutron scattering data at $T = 100$ K [1] together with the associated error bars are shown as filled diamonds.

the SR and FR Fermi surfaces do not differ qualitatively and are in good agreement with the experimental measurements of Anderson and Gold [31].

The anomaly of the L branch along Σ is shown in figure 5. This anomaly has been found in almost all previous SR linear response calculations and it is visible also when the phonons are calculated by a frozen phonon technique [19]. The anomaly appears around the vector $\mathbf{q} = (0.32, 0.32, 0)$ and has been explained as a Kohn anomaly with the nesting vector $\mathbf{v}_1$ shown

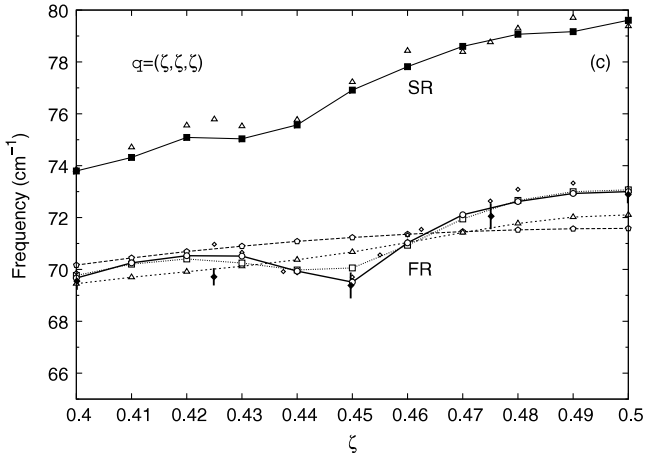

Figure 6. Enlarged view of the FR phonon dispersion of the L branch close to the point $\mathbf{q} = (0.45, 0.45, 0.45)$ (square (c) in figure 3) along the Λ line. $\sigma = 0.1$ Ryd (pentagons), $\sigma = 0.05$ Ryd (triangles), $\sigma = 0.02$ Ryd (squares), $\sigma = 0.01$ Ryd $N_k = 40$ (circles) $\sigma = 0.01$ $N_k = 32$ (small empty diamonds). Neutron scattering data at $T = 100$ K [1], together with the associated error bars, are shown as filled diamonds. The SR points are obtained with $\sigma = 0.01$ Ryd and $N_k = 40$ (filled squares) and $N_k = 32$ (triangles).

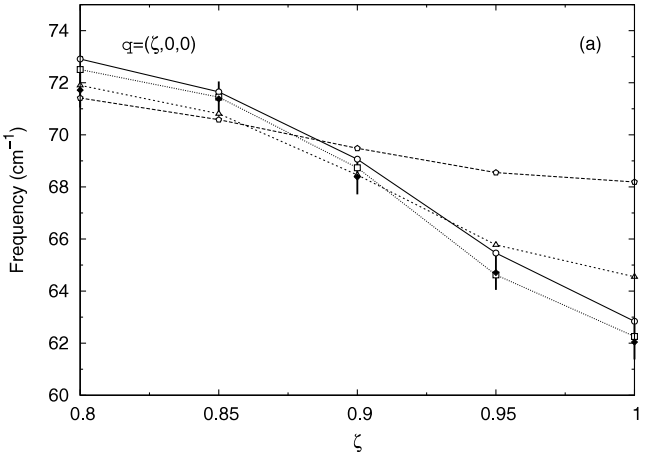

Figure 7. Enlarged view of the FR phonon dispersion of the L branch close to the X point along the Δ line. The dispersions are calculated with different values of the smearing parameter σ which controls the sharpness of the Fermi surface. $\sigma = 0.1$ Ryd (pentagons), $\sigma = 0.05$ Ryd (triangles), $\sigma = 0.02$ Ryd (squares), $\sigma = 0.01$ Ryd (circles). Neutron scattering data at $T = 100$ K [1], together with the associated error bars, are shown as filled diamonds.

in figure 4 which joins two flat regions of the Fermi surface [1]. In our calculation the radius of the Fermi surface at the points connected by the vector $\mathbf{v}_1$ is 4% smaller than the radius of the free electron Fermi sphere. The position of the anomaly is in good agreement with this figure. The shape of the anomaly depends on the smearing parameter that controls the sharpness of the Fermi surface and actually the anomaly disappears for $\sigma = 0.05$ and 0.1 Ryd. Therefore a well defined Fermi surface is necessary for its description as expected for a Kohn anomaly.

The anomaly of the L branch along Λ is shown in figure 6. This anomaly has been explained with the nesting vector $\mathbf{v}_2$ [1] shown in figure 4. Like the previous one, this anomaly is not found when the smearing parameter is $\sigma = 0.05$ or 0.1 Ryd. In this direction the radius of the FR Fermi surface is 1.5% larger than the radius of the free electron sphere corresponding to a vector $\mathbf{q} = (0.45, 0.45, 0.45)$ in agreement with the position of the anomaly. The SR Fermi surface has the same shape of the FR Fermi surface, with a radius, in this direction, 1% larger than the free electron sphere. Hence the SR dispersion curve should have an anomaly at a vector $\mathbf{q} = (0.44, 0.44, 0.44)$. This anomaly was not studied in previous papers so I have recalculated it with the SR-PP. Figure 6 shows that the anomaly is present also in the SR case although with a slightly different position and shape. Its position is compatible with the vector $\mathbf{q}$ deduced from the Fermi surface. The shape of the anomaly converged on this scale of frequencies is quite difficult to obtain. For $\sigma = 0.01$ Ryd, I have calculated the phonon frequencies with N_k up to 40 the value used in the figure. In the same figure the points obtained for $N_k = 32$ and $\sigma = 0.01$ Ryd are also shown in order to illustrate the convergence of the results with respect to the **k**-point sampling.

The dip of the L branch along Δ close to the zone-boundary point X is shown in figure 7. The dispersion has been calculated for the same values of σ as were used above. Changing σ from 0.01 to 0.1 Ryd, the frequency of the L phonon at X increases by about 5 cm^{-1}. The dip of the L branch at X behaves like the other two anomalies and is quite dependent on the sharpness of the Fermi surface, although even with the largest smearing parameter it does not disappear completely. The T branch at X instead increases only of 3 cm^{-1} passing from $\sigma = 0.01$ to 0.1 Ryd.

In closing, I make some comments on the accuracy of the result. The agreement between theory and experiment found in this paper is very satisfying but it is probably partly fortuitous, and could be spoiled by unavoidable systematic errors. Actually, in a plane wave pseudopotential phonon calculation there are several sources of uncertainties larger than the numerical error quoted above. The LDA is expected to be a good approximation for a nearly free electron system such as Pb but it could introduce errors much larger than 1 cm^{-1}. Actually for some difficult metals it has been found to give discrepancies as large as 10 cm^{-1} or more [19, 32]. Moreover, the PP approximation and the transferability properties of the PP are a major source of errors on the frequency scales analyzed in this paper. Uncertainties of a few cm^{-1} are quite common. The calculated phonon dispersions of fcc-Pb with a FR US-PP show that, within the LDA, the inclusion of spin–orbit coupling lowers the phonon frequencies with respect to a SR-PP. I have shown that the main anomalies present in the phonon dispersions are reproduced by the theory. Three of them have been calculated for different values of the smearing parameter that controls the sharpness of the Fermi surface and have been shown to reduce or disappear for large values of this parameter, so their interpretation as Kohn anomalies is further supported.

Acknowledgments

This work was supported by PRIN Cofin 2006022847, as well as by INFM/CNR ‘Iniziativa trasversale calcolo parallelo’. All

calculations were performed on the SISSA-Linux cluster and at CINECA in Bologna, by using the PWscf and PHONON codes, contained in the quantum-ESPRESSO package [33].

References

[1] Brockhouse B N, Arase T, Caglioti G, Rao K R and Woods A D B 1962 *Phys. Rev.* **128** 1099
[2] Kohn W 1959 *Phys. Rev. Lett.* **2** 393
[3] Aynajian P, Keller T, Boeri L, Shapiro S M, Habicht K and Keimer B 2008 *Science* **319** 1509
[4] Vosko S H, Taylor R and Keech G H 1965 *Can. J. Phys.* **43** 1187
[5] Bertoni C M, Bortolani V, Calandra C and Nizzoli F 1974 *J. Phys. F: Met. Phys.* **4** 19
[6] Wang Y R and Overhauser A W 1987 *Phys. Rev.* B **35** 501
[7] Lynn J W, Smith H G and Nicklow R M 1973 *Phys. Rev.* B **8** 3493
[8] Dutton D H, Brockhouse B N and Miiller A P 1972 *Can. J. Phys.* **50** 2915
[9] Brockhouse B N, Rao K R and Woods A D B 1961 *Phys. Rev. Lett.* **7** 93
[10] Chen X M and Overhauser A W 1989 *Phys. Rev.* B **39** 10570
[11] So C B, Moore R A and Wang S 1978 *J. Phys. F: Met. Phys.* **8** 785
[12] de Gironcoli S 1995 *Phys. Rev.* B **51** 6773
[13] Savrasov S Y and Savrasov D Y 1996 *Phys. Rev.* B **54** 16487
[14] Liu A Y and Quong A A 1996 *Phys. Rev.* B **53** R7575
[15] Baroni S, Giannozzi P and Testa A 1987 *Phys. Rev. Lett.* **58** 1861
Giannozzi P, de Gironcoli S, Pavone P and Baroni S 1991 *Phys. Rev.* B **43** 7231
Dal Corso A 2001 *Phys. Rev.* B **64** 235118
[16] Bachelet G B, Hamann D R and Schlüter M 1982 *Phys. Rev.* B **26** 4199
[17] Koelling D D and Harmon B N 1977 *J. Phys. C: Solid State Phys.* **10** 3107
[18] Louie S G, Froyen S and Cohen M L 1982 *Phys. Rev.* B **26** 1738
[19] Grabowski B, Hickel T and Neugebauer J 2007 *Phys. Rev.* B **76** 024309
[20] Dal Corso A 2007 *Phys. Rev.* B **76** 054308
[21] Vanderbilt D 1990 *Phys. Rev.* B **41** 7892
[22] Rappe A M, Rabe K M, Kaxiras E and Joannopoulos J D 1990 *Phys. Rev.* B **41** 1227
[23] Kresse G and Hafner J 1994 *J. Phys.: Condens. Matter* **6** 8245
[24] Dal Corso A and Mosca Conte A 2005 *Phys. Rev.* B **71** 115106
[25] Perdew J and Zunger A 1981 *Phys. Rev.* B **23** 5048
[26] Methfessel M and Paxton A T 1989 *Phys. Rev.* B **40** 3616
[27] Gonze X and Lee C 1997 *Phys. Rev.* B **55** 10355
[28] Vohra Y K and Ruoff A L 1990 *Phys. Rev.* B **42** 8651
[29] Yu D and Scheffler M 2004 *Phys. Rev.* B **70** 155417
[30] Liu A Y, García A, Cohen M L, Godwal B K and Jeanloz R 1991 *Phys. Rev.* B **43** 1795
[31] Anderson J R and Gold A V 1965 *Phys. Rev.* A **139** 1459
[32] Favot F and Dal Corso A 1999 *Phys. Rev.* B **60** 11427
[33] Giannozzi P *et al* http://www.quantum-espresso.org